The Inductive Susceptance Observed with Electrode Reaction of Water at Far Negative Potentials

Katsuo TAKAHASHI, Kiyoshi MATSUDA, and Reita TAMAMUSHI

The Institute of Physical and Chemical Research, Hirosawa, Wako, Saitama 351

(Received July 16, 1975)

The admittance of various electrodes/dilute aqueous electrolyte solution systems was measured at far negative potentials in the frequency range of 22—500 Hz, and the experimental results were discussed in terms of the mechanism of the electrochemical reduction of water molecules. The frequency dependence of the conductance- and susceptance-components was analyzed by assuming possible equivalent circuits. It was concluded that, in the systems which give inductive susceptances at low frequencies, the reduction of water proceeds according to the electrochemical mechanisms;

$$H_2O + e \longrightarrow H_{ad} + OH^-, \quad H_{ad} + H_2O + e \longrightarrow H_2 + OH^-$$

where the current density due to the second reaction path is proportional to the product of θ and $(1-\theta)$, θ being the coverage of the electrode surface by adsorbed hydrogen atoms, H_{ad}. At some metal electrodes in solutions of alkali-metal cations, no inductive susceptance was observed; this suggests that the hydrogen evolution proceeds according to other mechanisms.

The faradaic admittance of usual electrode reactions involves a positive conductance and a capacitive susceptance. In some electrode reactions, however, unusual faradaic admittances with negative conductances and/or inductive susceptances have been observed under certain experimental conditions. A typical example with a negative conductance is the reduction of In(III) at a dropping mercury electrode (DME) in thiocyanate solutions,[1] while an example with an inductive susceptance is the electrochemical dissolution of iron and nickel in alkaline solutions.[2] The theoretical interpretation of these unusual faradaic admittances has been made by several authors[1-6] in connexion with the mechanisms of electrode reactions; in particular, a recent study of Smith and Sobel[5] clearly demonstrates the possibility of some ECE mechanisms giving inductive susceptances.

In the cathodic evolution of hydrogen, the appearance of an inductive susceptance was suggested on a theoretical basis by Gerischer and Mehl,[3] by Batrakov and Iofa,[7] and by Novosel'skii and Gudina.[8] In a previous paper,[9] the present authors reported the experimental observation that the susceptance components of DME/dilute aqueous electrolyte solutions become inductive at far negative potentials, where the reduction of water molecules is supposed to proceed. This paper will present the details of the admittance behavior of the above-mentioned systems and will discuss the possible mechanism of the electrochemical reduction of water molecules.

Experimental

The electrolytic currents (DC-components), conductances, and susceptances due to the electrode process were measured as functions of the electrode potential by using an apparatus whose block diagram is shown in Fig. 1; the instrumental details of the apparatus were reported previously.[10] The readings of each output-signal of the instrument were carefully calibrated by using appropriate dummy cells consisting of known resistors and capacitors. The output-signal of the 90°-phase-sensitive-detector at the stage before a low-pass filter, when observed with a cathode-ray oscilloscope, gives the patterns shown in Fig. 2 according to the nature of the admittance to be measured; this difference in the oscilloscopic patterns was used to determine whether the susceptance component was capacitive or inductive.

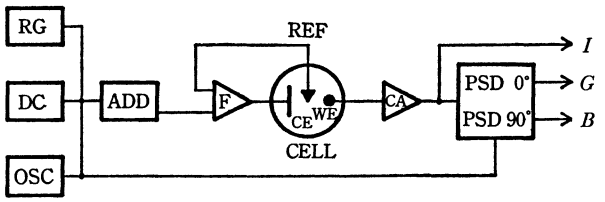

Fig. 1. Block diagram of the measuring instrument. RG: ramp-generator; DC: DC-voltage source; OSC: oscillator; ADD: adder; F: follower-type potentiostat; CA: current amplifier; PSD: phase-sensitive detector.

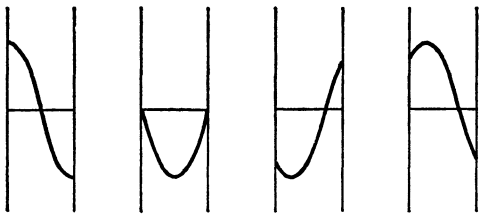

Fig. 2. Typical oscilloscopic patterns observed at the output of the 90°-PSD (before the low-pass filter) when the admittance to be measured (a) pure resistance, (b) pure capacitance, (c) capacitive admittance, (d) inductive admittance.

The arrangement of electrodes (working, counter, and reference electrodes) in a cell was the same as that described in a previous paper.[11] Conventional DME and microelectrodes (both rotating and stationary) of various metals were used as the working electrodes; in the case of the DME, the rate of the flow of the mercury was 0.526 mg s^{-1}, the drop time was mechanically controlled at 4.1 s, and admittance measurements were made at a surface area of 0.0142 cm^2. The counter electrode was a Pt-Pt spiral with large dimensions. In most solutions a Pt-Pt spiral was employed as the reference electrode; in chloride solutions, however, a Ag-AgCl electrode was also used as the reference. In this paper, the electrode potential is not corrected for the ohmic *IR*-drop.

All the solutions were prepared from analytical reagent-

grade chemicals by using redistilled water. The measurements were carried out with deaerated solutions at 25.0± 0.1 °C.

Results

The direct current (I)-potential (E), conductance (G)-E, and susceptance (B)-E curves observed with a DME/0.5 mM $Cd(NO_3)_2$ system were given in a previous paper;[9] the B-E curve clearly shows the inductive susceptance ($B<0$) at very negative potentials, where the cathodic current, which is considered to be due to the reduction of water molecules,[12] increases almost linearly with the electrode potential. Similar inductive susceptances were also observed at the DME in solutions containing various cations and at many solid electrodes in dilute aqueous solutions of strong acids; the systems examined in this work are summarized in Table 1.

Figures 3, 4, and 5 present typical examples of the I-E, G-E, and B-E curves obtained with the DME/1 mM KNO_3, Pt/2 mM HCl, and Pt/1 mM NaCl systems

Table 1. Appearance of the inductive susceptance in various electrode/solution systems at far negative potentials

Electrode	Inductive susceptance ($B<0$)	
	Observed in solutions containing	Not observed in solutions containing
Hg (DME)	Ag(I), Hg(I), Cd(II), Pb(II), Zn(II), Ni(II), In(III), H^+, Li^+, Na^+, K^+, Ca^{2+}, Al^{3+}	Mg^{2+}, tetraalkylammonium ions
Pt, Cu, Cd, Pb, Sn, Ni, Ti, W, graphite	H^+ (strong acids)	alkali metal cations, NH_4^+, Mg^{2+}
Ag	H^+ ($HClO_4$)	H^+ (HCl)

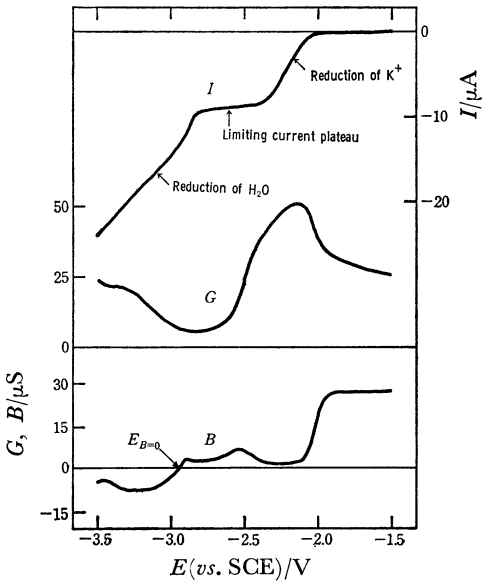

Fig. 3. I-E, G-E, and B-E curves observed at a DME in a 1 mM KNO_3 solution of 25 °C; the admittance being measured at 31 Hz.

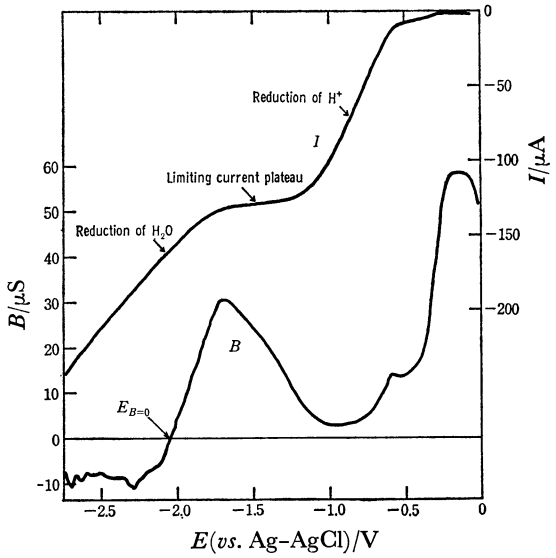

Fig. 4. I-E and B-E curves observed at a Pt-electrode in a 2 mM HCl solution of 25 °C; admittance being measured at 64 Hz.

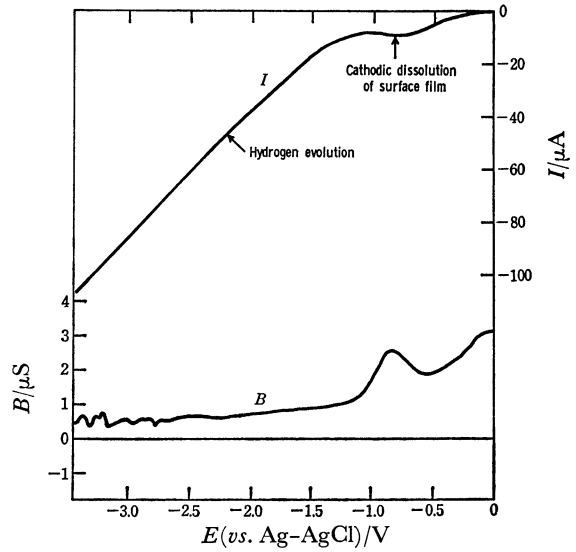

Fig. 5. I-E and B-E curves observed at a Pt-electrode in a 1 mM NaCl solution of 25 °C; admittance being measured at 64 Hz.

respectively. In the systems which give inductive susceptances at far negative potentials, the cathodic limiting-current plateau due to the reduction of the cations in the solution is clearly observed on the I-E curve, and the final rise in the cathodic current is well separated from the previous reduction step of the cation (see Figs. 3 and 4). On the other hand, no inductive susceptances could be observed at many solid electrodes in aqueous solutions containing alkali-metal cations; in these systems, the cathodic current increases monotonously without reaching a limiting-current plateau (see Fig. 5). The following part of this paper will be concerned mainly with the inductive susceptances observed with the DME systems.

The electrode potentials, $E_{B=0}$, where the susceptance, B, changes from capacitive ($B>0$) to inductive ($B<0$),

Table 2. Electrode potential, $E_{B=0}$, observed with DME/nitrate solutions of various cations; measured at 31 Hz and at 25 °C

Cation	$E_{B=0}$ V(*vs.* SCE)	$E_{1/2}$[a] V(*vs.* SCE)
Pb(II)	−1.9	−0.4
Cd(II)	−1.9	−0.6
Zn(II)	−1.9	−1.1
Ni(II)	−1.9	−1.1
Ag^+	−2.3	>0
Hg(I)	−2.3[b]	>0
In(III)	−2.3	−1.0
H^+	−2.5	−1.6
Al^{3+}	−2.6	−1.7
Na^+	−2.8	−2.1
K^+	−3.0	−2.1
Li^+	−3.1	−2.3
Ca^{2+}	−3.2	−2.2

a) Approximate values. b) In a perchlorate solution.

are summarized in Table 2. As may be seen from this table, the cations can be classified into two groups according to the correlation between their $E_{B=0}$ and their polarographic half-wave potentials, $E_{1/2}$: Group (A) includes the cations (Pb^{2+}, Cd^{2+}, Zn^{2+}, Ni^{2+}, Ag^+, Hg_2^{2+}, and In^{3+}), whose half-wave potentials are less negative than that of H^+; Group (B) includes the cations (Li^+, Na^+, K^+, Ca^{2+}, and Al^{3+}), whose half-wave potentials are more negative than that of H^+. The $E_{B=0}$ values for the cations in Group (A) do not show any particular correlation with the half-wave potentials, while the $E_{B=0}$ values for the cations in Group (B) become more negative in the same order as their half-wave potentials.

The effect of the frequency on the inductive susceptance was studied mainly with DME/KNO_3 (or KCl) solutions. The electrode potential, $E_{B=0}$, for a DME/1 mM KNO_3 system shifted to more negative potentials almost linearly with the increasing frequency, as is shown in Fig. 6. The $E_{B=0}$ value extrapolated to zero frequency was found to be equal to the electrode potential, E_D, where the polarographic cathodic current begins to increase linearly with the electrode potential (see Fig. 6).

The frequency dependence of the admittance measured with a DME/1 mM KNO_3 system at several electrode potentials is shown in Fig. 7 by plotting B against G on a complex admittance plane. Similar diagrams were also obtained with DME/KCl solutions of different concentrations at $E=-3.2$ V (*vs.* SCE) (see Fig. 8). The *B-G* plots for these systems suggest that the electric properties of the systems can be represented by assuming some resonance circuits which involve capacitive and inductive elements.

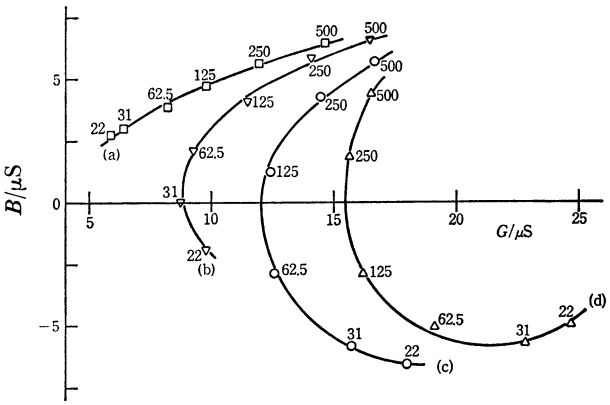

Fig. 7. Frequency dependence of the admittance measured with a DME/1 mM KNO_3 system at different electrode potentials; E/V(*vs.* SCE) = −2.8(a), −3.0 (b), −3.2(c), and −3.4(d). The figure beside each experimental point represents the frequency in Hz.

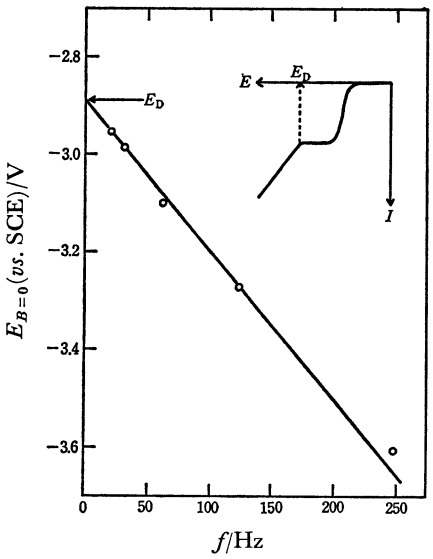

Fig. 6. Frequency dependence of $E_{B=0}$ of a DME/1 mM KNO_3 system at 25 °C.

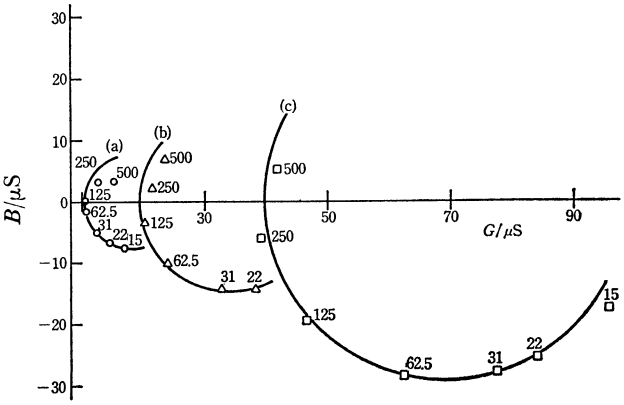

Fig. 8. Frequency dependence of the admittance measured with a DME/KCl system at different concentrations of KCl and at $E=-3.2$ V(*vs.* SCE): (a) 1 mM, (b) 2 mM, and (c) 4 mM KCl. The figure beside each experimental point represents the frequency in Hz.

Discussion

The experimental results presented in the previous section suggest that the appearance of the inductive susceptance is related to the mechanism of the reduction process of water molecules at the electrodes.

In analogy with the mechanisms proposed for the hydrogen overvoltage,[13] water molecules are considered to be reduced electrochemically through either one of the following reaction schemes: the recombination (EC) mechanism (I):

$$H_2O + e \rightarrow H_{ad} + OH^- \quad \text{(I-1)}$$

$$H_{ad} + H_{ad} \rightarrow H_2 \quad \text{(I-2)}$$

or the electrochemical (EE′ or ECE′) mechanism (II):

$$H_2O + e \rightarrow H_{ad} + OH^- \quad \text{(II-1)}$$

$$H_{ad} + H_2O + e \rightarrow H_2 + OH^- \quad \text{(II-2)}$$

where H_{ad} indicates the hydrogen atom adsorbed on the electrode surface. In solutions containing alkali-metal cations, a third (catalytic) mechanism (III) can be considered, in which the reduction of water molecules proceeds *via* an intermediate discharge of alkali-metal cations:

$$M^+ + e(Me) \rightarrow M(Me) \quad \text{(III-1)}$$

$$M(Me) + H_2O \rightarrow M^+ + H_{ad} + OH^- + (Me) \quad \text{(III-2)}$$

$$H_{ad} + H_{ad} \rightarrow H_2 \quad \text{(III-3)}$$

where M^+ is an alkali-metal cation and Me represents a metal of the electrode.

According to the theoretical analysis of the faradaic admittance by Smith and Sobel,[5] no faradaic susceptance of the inductive nature can be expected for the electrode reactions with the following mechanisms: a simple charge-transfer process, the CE and EC mechanisms, and a catalytic mechanism, unless negative transfer-coefficients are assumed. In the cases of the ECE′ and $(EC)_nE'$ mechanisms, however, the theory shows that inductive susceptances can be observed under certain conditions. This theoretical result suggests that the inductive susceptance in our present systems can be explained more reasonably by assuming the electrochemical mechanism (II) than by assuming the recombination mechanism (I) or the mechanism (III) for the reduction of water molecules.

Theoretical Expressions for the Faradaic Admittance. In this paper, the theoretical expressions of the faradaic admittance for the reaction mechanism (II) are derived on the basis of the following assumptions*:

(a) In the negative potential region where the cathodic current due to the reduction of water molecules is observed, the partial anodic current can be neglected in comparison with the partial cathodic current. Thus, the overall faradaic current density (c.d.), j, due to the reaction (II) is given by:

$$j = j_{c1} + j_{c2} \quad (1)$$

where j_{c1} and j_{c2} are the partial cathodic c.d. for the reaction steps (II-1) and (II-2) respectively.

(b) The partial cathodic c.d., j_{c1}, is represented by:

$$j_{c1}/F = -k_1(1-\theta)\exp(-\beta_1 E) \quad (2)$$

with

$$\beta_1 = \frac{\alpha_{c1}F}{RT} \quad (3)$$

where θ is that fraction of the electrode surface which is covered with H_{ad}; E, the electrode potential referred to a given reference electrode; α_{c1}, the cathodic transfer-coefficient for the step (II-1); k_1, a positive constant which is independent of E, and θ but a function of the concentration of H_2O at the electrode surface. The other symbols have their usual meanings. In this paper, the sign of the cathodic current is taken as negative.

(c) The partial cathodic c.d., j_{c2}, is given by:

$$j_{c2}/F = -k_2\theta(1-\theta)\exp(-\beta_2 E) \quad (4)$$

with

$$\beta_2 = \frac{\alpha_{c2}F}{RT} \quad (5)$$

where α_{c2} is the cathodic transfer-coefficient for the step (II-2), and k_2, a positive constant similar to k_1.

Some authors[2,7,8] have used the expression:

$$j_{c2}/F = -k_2\theta\exp(-\beta_2 E) \quad (4')$$

As will be discussed later, however, Eq. (4′) cannot explain the present experimental results. Therefore, the following analysis will be made primarily on the basis of Eq. (4).

(d) Under the experimental conditions of the admittance measurement, the electrode potential, E, is equal to the sum of a DC-component, $\bar{E}$, and an AC-component, $\tilde{E}$:

$$E = \bar{E} + \tilde{E} \quad (6)$$

The AC-component is assumed to be sufficiently small, so that the condition:

$$\exp(-\beta_{1(2)}\tilde{E}) = 1-\beta_{1(2)}\tilde{E} \quad (7)$$

is satisfied.

For the faradaic c.d. and for the coverage, we assume the following relations, respectively:

$$j = \bar{j} + \tilde{j} = (\bar{j}_{c1}+\bar{j}_{c2}) + (\tilde{j}_{c1}+\tilde{j}_{c2}) \quad (8)$$

and

$$\theta = \bar{\theta} + \tilde{\theta} \quad (9)$$

where $\bar{j}$ and $\bar{\theta}$ are the DC-components, and $\tilde{j}$ and $\tilde{\theta}$, the AC-components.

(e) When $\tilde{E}$ is given by

$$\tilde{E} = \Delta E\exp(j\omega t) \quad (10)$$

$\tilde{\theta}$ is represented by

$$\tilde{\theta} = \Delta\theta\exp(j\omega t+\phi) \quad (11)$$

where ΔE and $\Delta\theta$ are the amplitudes; ω, the angular frequency; ϕ, the phase-angle between $\tilde{E}$ and $\tilde{\theta}$, and t, the time.

(f) The contribution of the time-dependence of the H_2O-concentration at the electrode surface to the

* Similar treatments of the faradaic admittance have been reported by Batrakov and Iofa,[7] by Novosel'skii and Gudina,[8] and by Epelboin *et al.*[2]

faradaic admittance can be ignored, because a large amount of H_2O is available for the reaction.

By using these assumptions and by neglecting the terms involving a product of the AC-components (*e.g.*, $\tilde{\theta}\tilde{E}$), we obtain the following expressions for $\bar{j}$ and $\tilde{j}$:

$$-\bar{j}/F = (1-\bar{\theta})(\bar{k}_1+\bar{k}_2\bar{\theta}) \tag{12}$$

and

$$\tilde{j}/F = \{\bar{k}_1+\bar{k}_2(2\bar{\theta}-1)\}\tilde{\theta} + (1-\bar{\theta})(k_1\beta_1+k_2\bar{\theta}\beta_2)\tilde{E} \tag{13}$$

where

$$\bar{k}_1 = k_1\exp(-\beta_1\bar{E}) \text{ and } \bar{k}_2 = k_2\exp(-\beta_2\bar{E}) \tag{14}$$

The faradaic admittance, Y_F, is then given by the equation:

$$Y_F = G_F + jB_F = \frac{d\bar{j}}{d\tilde{E}} = F(1-\bar{\theta})(\bar{k}_1\beta_1+\bar{k}_2\bar{\theta}\beta_2) + F\{\bar{k}_1+\bar{k}_2(2\bar{\theta}-1)\}\frac{d\tilde{\theta}}{d\tilde{E}} \tag{15}$$

where G_F is the faradaic conductance, and B_F, the faradaic susceptance.

The time-dependence of the coverage, θ, follows the relation:

$$[H_{ad}]_s\frac{d\theta}{dt} = k_1(1-\theta)\exp(-\beta_1E) - k_2\theta(1-\theta)\exp(-\beta_2E) \tag{16}$$

where $[H_{ad}]_s$ is the maximum amount of H_{ad} divided by the surface area of the electrode when the surface is saturated with H_{ad}. Similarly to the faradaic c.d., $d\theta/dt$ can be divided into the DC- and AC-components:

$$[H_{ad}]_s\frac{d\bar{\theta}}{dt} = (1-\bar{\theta})(\bar{k}_1-\bar{k}_2\bar{\theta}) \tag{17}$$

and

$$[H_{ad}]_s\frac{d\tilde{\theta}}{dt} = -\{\bar{k}_1+\bar{k}_2(1-2\bar{\theta})\}\tilde{\theta} - (1-\bar{\theta})(\bar{k}_1\beta_1-\bar{k}_2\bar{\theta}\beta_2)\tilde{E} \tag{18}$$

The introduction of Eq. (11) into Eq. (18) gives the equation for $d\tilde{\theta}/d\tilde{E}$:

$$\frac{d\tilde{\theta}}{d\tilde{E}} = -\frac{(1-\bar{\theta})(\bar{k}_1\beta_1-\bar{k}_2\bar{\theta}\beta_2)}{\bar{k}_1+\bar{k}_2(1-2\bar{\theta})+j\omega[H_{ad}]_s} \tag{19}$$

From Eqs. (15) and (19), the following expressions are derived for the faradaic conductance and susceptance respectively:

$$G_F = G_F' + G_F'' \tag{20}$$

$$G_F' = F(1-\bar{\theta})(\bar{k}_1\beta_1+\bar{k}_2\bar{\theta}\beta_2) \tag{21}$$

$$G_F'' = \frac{q}{1+\omega^2p^2} \tag{22}$$

$$B_F = \frac{-\omega pq}{1+\omega^2p^2} \tag{23}$$

where

$$p = \frac{[H_{ad}]_s}{\bar{k}_1+\bar{k}_2(1-2\bar{\theta})} \tag{24}$$

and

$$q = -F\frac{\bar{k}_1-\bar{k}_2(1-2\bar{\theta})}{\bar{k}_1+\bar{k}_2(1-2\bar{\theta})}(1-\bar{\theta})(\bar{k}_1\beta_1-\bar{k}_2\bar{\theta}\beta_2) \tag{25}$$

The conductance, G_F', being independent of the frequency, is equivalent to the reciprocal of the charge-transfer resistance, while the conductance, G_F'', and the susceptance, B_F, both being dependent on the frequency, are due to the concentration polarization.

Equation (21) shows that G_F' is always positive if both the transfer-coefficients, α_{c1} and α_{c2}, are positive (*i.e.*, $\beta_1>0$ and $\beta_2>0$). In our present systems, the possibility of negative transfer-coefficients may be excluded because of the normal behavior of the DC *I-E* curves (if the transfer-coefficient were negative, some abnormal decrease in the cathodic current could be observed with the increase in the negative potentials).

In order to discuss the conditions under which the faradaic susceptance becomes inductive ($B_F<0$), the stationary-state assumption is introduced with respect to the DC-component of the coverage: $d\bar{\theta}/dt=0$. By using this assumption, we obtain the relation:

$$\bar{k}_1 = \bar{k}_2\bar{\theta} \tag{26}$$

from Eq. (17) unless $(1-\bar{\theta})=0$.

From Eqs. (21), (24), (25), and (26), the following expressions are derived for p and a dimensionless parameter, r, which is the ratio of q to G_F':

$$p = \frac{[H_{ad}]_s}{\bar{k}_2(1-\bar{\theta})} \tag{27}$$

and

$$r \equiv \frac{q}{G_F'} = \frac{(3\bar{\theta}-1)(1-b)}{(1-\bar{\theta})(1+b)} \tag{28}$$

where b is a dimensionless quantity as defined by

$$b \equiv \frac{\beta_1}{\beta_2} = \frac{\alpha_{c1}}{\alpha_{c2}} \tag{29}$$

When $r>0$, q must be positive and the faradaic susceptance, B_F, becomes inductive ($B_F<0$), because p should be positive according to Eq. (27). On the other hand, if $r<0$, q must be negative and the faradaic susceptance becomes capacitive ($B_F>0$). By means of Eq. (28), the relationship between b and $\bar{\theta}$ can be drawn for different values of r, as is shown in Fig. 9; (a) represents the b-$\bar{\theta}$ diagram for $r>0$ (inductive susceptance), and (b), the b-$\bar{\theta}$ diagram for $r<0$ (capacitive susceptance). In Fig. 9(a), the combination of b and $\bar{\theta}$ which will result in an inductive susceptance under the condition, $b>0$, is shown by solid lines.

The above theoretical treatment of the faradaic admittance, although not very rigorous, clearly demonstrates that the susceptance, B_F, for the electrochemical mechanism (II) can be either capacitive or inductive according to the conditions determined by the r, b, and $\bar{\theta}$ parameters (see Fig. 9(a) and (b)).

Complex Admittance Plane Diagram and the Equivalent Circuit. Equations (20)—(23) for the faradaic conductance and susceptance show that, when $q>0$,

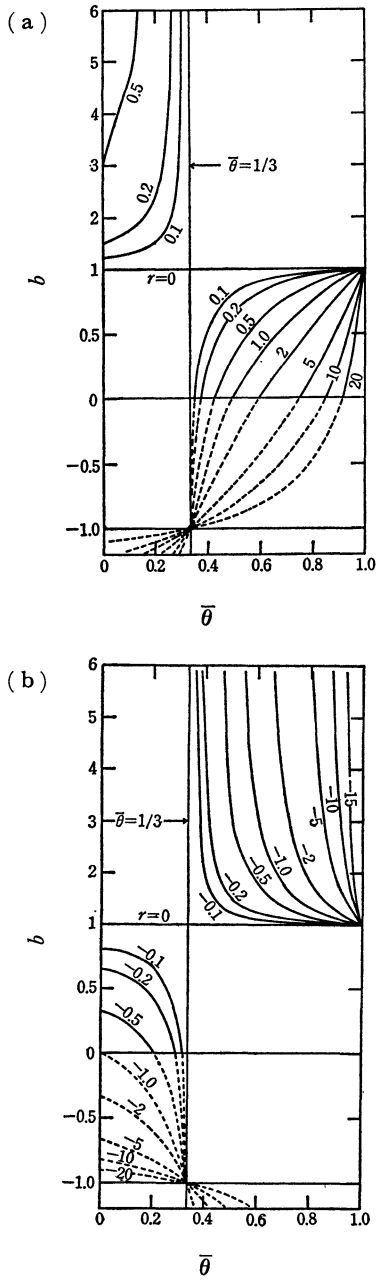

Fig. 9. Theoretical b-$\bar{\theta}$ curves for various values of the parameter, r, as calculated by means of Eq. (28): (a), b-$\bar{\theta}$ curves for $r>0$ (inductive susceptance); (b), b-$\bar{\theta}$ curves for $r<0$ (capacitive susceptance). Solid lines correspond to the condition, $b>0$, and broken lines to the condition, $b<0$.
The figure beside each curve represents the r-value.

a plot of B_F against G_F on a complex admittance plane gives a semi-circle with its center at $[(G_F')+(q/2)]$ and a radius of $q/2$, as is shown in Fig. 10. This admittance behavior can be represented by assuming an equivalent circuit which consists of two resistances, R_1 and R_2, and an inductance, L, as is presented in Fig. 10(a), where $R_1=(G_F')^{-1}$, $R_2=q^{-1}$, $r=R_1/R_2$, $L=p/q$, and the time-constant of the circuit is equal to L/R_2 $(=p)$.

The conductance and the susceptance of an electrode/solution system, which can be measured experimentally,

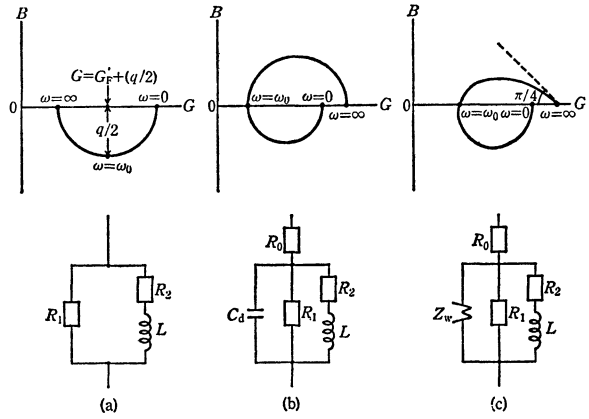

Fig. 10. Theoretical B-G plots (schematic) on a complex admittance plane and the corresponding equivalent circuits.

involve not only the faradaic components, but also the solution resistance, R_0, and the double-layer capacity, C_d. It has been shown by our previous studies[11,14] that, in the far negative potential region where the reduction of all the cations present in the solution gives the cathodic limiting-current plateau, the double-layer capacity of the Helmholtz-Gouy-Chapmann type becomes very small and the admittance behavior of the electrode surface is practically determined by the Warburg-type impedance, Z_w, due to the mass-transport of the depolarizable cations. Consequently, the actual equivalent circuit for the system which gives inductive susceptances may be considered to be represented either by (b) or (c) in Fig. 10; the schematical B-G plots corresponding to the equivalent circuits are presented in the same figure. The expressions for the characteristic points on the complex admittance plane are summarized in Table 3.

Both the equivalent circuits, (b) and (c), can reproduce the experimental observation that the B-G plot starts from the fourth quadrant of the complex admittance plane at lower frequencies and then passes into the first quadrant with the increase in the frequency (see Figs. 7 and 8). In Fig. 11, one of the best experimental results is compared with the B-G diagrams obtained by means of simulation using the equivalent circuits (b) and (c) in Fig. 10; the values of each element, as determined by simulation, are summarized in Table 4. The values of r thus obtained are relatively large, suggesting that the possible values of $\bar{\theta}$ should be in the range of $0.8<\bar{\theta}<1$ (see Fig. 9(a)); in other words, $\bar{k}_2$ is close to $\bar{k}_1$, according to relation (26).

Finally, let us discuss the possibility that the current density due to the reaction path (II-2) is given by Eq. (4'). In this case, too, inductive susceptances can be expected when $r>0$; by following a similar treatment, we obtain the b-$\bar{\theta}$ diagram shown in Fig. 12 for various positive values of r. Figure 12 suggests that the values of r cannot be larger than unity $(r<1)$ for the appearance of inductive susceptances. This result is not in agreement with the r-values ($r=15$ or 25) evaluated by means of simulation (see Table 4).

Table 3. Expressions for the characteristic points on the *B-G* plot in terms of the equivalent circuits given in Fig. 10

Characteristic point	Expression in terms of the equivalent circuit (a)	(b)	(c)[a]
$G(\omega=0)$	$\frac{1}{R_1}+\frac{1}{R_2}$	$\frac{1}{R_0+\left(\frac{1}{R_1}+\frac{1}{R_2}\right)^{-1}}$	$\frac{1}{R_0+\left(\frac{1}{R_1}+\frac{1}{R_2}\right)^{-1}}$
$G(\omega=\infty)$	$\frac{1}{R_1}$	$\frac{1}{R_0}$	$\frac{1}{R_0}$
$G(\omega=\omega_0)$	$\frac{1}{R_1}+\frac{1}{2R_2}$	$\frac{1}{R_0+\left\{\frac{1}{R_1}+\frac{1}{R_2}\left(1+\frac{\omega_0^2L^2}{R_2^2}\right)^{-1}\right\}^{-1}}$	$\frac{1}{R_0+\left\{\frac{1}{R_1}+\frac{1}{2S}\left(\frac{R_2}{L\sqrt{\omega}_0}+\sqrt{\omega}_0\right)\right\}^{-1}}$
ω_0	$\omega_0=\frac{R_2}{L}$	$\omega_0^2=\frac{1}{LC_d}-\left(\frac{R_2}{L}\right)^2$	$\omega_0^2L^2-2SL\sqrt{\omega}_0+R_2^2=0$

a) The Warburg impedance is assumed to be given by $Z_w=S\omega^{-1/2}(1-j)$.

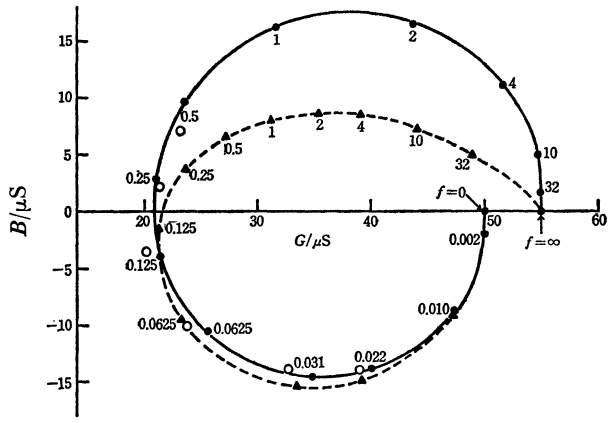

Fig. 11. Comparison of the simulated *B-G* diagrams with the experimental results obtained with a DME/2 mM KCl system at $E=-3.2$ V(*vs.* SCE): -●- and -▲-, simulated curves by using the equivalent circuits (b) and (c), respectively, in Fig. 10; ○, experimental points. The figure beside each point represents the frequency in kHz.

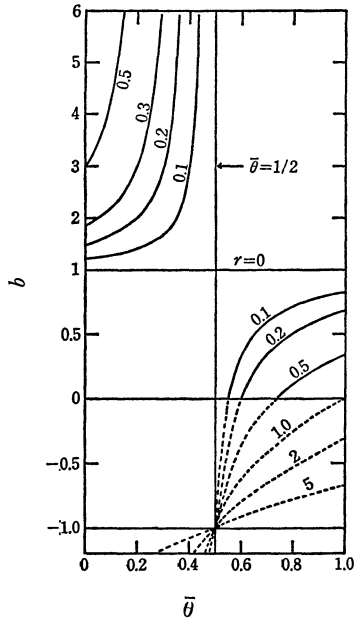

Fig. 12. Theoretical b-$\bar{\theta}$ curves for various positive values of r, as calculated by means of an equation which is derived on the basis of Eq. (4′). Solid lines correspond to the condition, $b>0$, and broken lines to the condition, $b<0$.

Table 4. The values of each element in the equivalent circuits given in Fig. 10, as determined by simulation (see Fig. 11)
System: DME/2 mM KCl; $E=-3.2$ V(*vs.* SCE); surface area of the DME, 0.0142 cm².

Equivalent circuit	R_0 kΩ	R_1 kΩ	R_2 kΩ	r	L H	C_d μF	S[a] kΩ s$^{-1/2}$
Fig. 10(b)	18	30	2	15	70	0.01	—
Fig. 10(c)	18	50	2	25	70	—	10^3

a) The Warburg impedance is assumed to be given by $Z_w=S\omega^{-1/2}(1-j)$; an approximate value of $S(S=10^3$ kΩ s$^{-1/2}$) was estimated from our previous work.[11]

Conclusion

The discussion above has been made on the basis of the assumption that the inductive susceptance is related to the mechanism of the faradaic processes. There may exist some other mechanisms of the non-faradaic nature which also give inductive susceptances at an electrode/solution interface. However, so long as we accept the above assumption, we can conclude that, in the electrode systems which show the inductive susceptance at far negative potentials, water molecules are reduced through the electrochemical mechanism (II), in which the rate of reaction path (II-2) is proportional to the product of θ and $(1-\theta)$.

The experimental fact that no inductive susceptance is observed at some metal electrodes in solutions containing alkali-metal cations (see Table 1) suggests the possibility that the hydrogen evolution proceeds according to the other mechanisms, such as (I) or (III), in such systems.

References

1) N. Tanaka, T. Takeuchi, and R. Tamamushi, This Bulletin, **37**, 1435 (1964); R. Tamamushi and K. Matsuda, *J. Electroanal. Chem.*, **12**, 436 (1966); B. Timmer and M. Sluyters-Rehbach, *ibid.*, **19**, 73 (1968); R. de Levie and A. A. Husovsky, *ibid.*, **22**, 29 (1969).

2) I. Epelboin, M. Keddam, and J. -C. Lestrade, *Revue Generale de l'electricite*, **76**, 777 (1967); R. Wiart, *Oberflach-Surface*, **9**, 213, 241, 275 (1968); I. Epelboin, and M. Keddam, *J. Electrochem. Soc.*, **117**, 1052 (1970).

3) H. Gerischer and W. Mehl, *Z. Elektrochem.*, **59**, 1049 (1955).

4) D. Schumann, *J. Electroanal. Chem.*, **17**, 45 (1968).

5) D. E. Smith and H. R. Sobel, *Anal. Chem.*, **42**, 1018 (1970).

6) R. de Levie, J. C. Kreuser, and H. Moreira, *ibid.*, **43**, 784 (1971).

7) V. V. Batrakov and Z. A. Iofa, *Elektrokhim.*, **1**, 123 (1965).

8) I. M. Novosel'skii and N. N. Gudina, *ibid.*, **5**, 820 (1969).

9) K. Matsuda, K. Takahashi, and R. Tamamushi, This Bulletin, **44**, 2880 (1971).

10) K. Matsuda, K. Takahashi, and R. Tamamushi, *Sci. Papers IPCR*, **64**, 62 (1970).

11) K. Takahashi and R. Tamamushi, This Bulletin, **48**, 3540 (1975).

12) D. Ilkovič, *Collection Czechoslov. Chem. Commun.*, **4**, 480 (1932); T. Okada and S. Yoshizawa, This Bulletin, **49**, 183 (1946); H. Imai and P. Delahay, *J. Phys. Chem.*, **66**, 1683 (1962).

13) A. N. Frumkin, "Advances in Electrochemistry and Electrochemical Engineering," Vol. 1 (P. Delahay, ed.) Interscience Publishers, New York (1961), pp. 65—121; A. Frumkin, V. Korshunov, and I. Bagozkaya, *Electrochim. Acta*, **15**, 289 (1970).

14) K. Takahashi and R. Tamamushi, *Electrochim. Acta*, **16**, 875, 1157 (1971).